Modelling Confocal and Offset Detection Paths of an AOSLO to Guide Contrast Optimization

Julia Granier,[1,2,*] Elena Gofas Salas,[1,2], Kate Grieve[1,2] and Peter Munro [3]

[1] *Sorbonne Université, INSERM, CNRS, Institut de la Vision, 17 rue Moreau, F-75012 Paris, France;*
[2] *CHNO des Quinze-Vingts, INSERM-DGOS CIC 1423, 28 rue de Charenton, F-75012 Paris, France*
[3] *University College London, Malet Place, Gower Street, London WC1E 6BT, UK*

[*] *julia.granier@inserm.fr*

Abstract: We present a model for confocal and offset aperture detection in an adaptive optics scanning laser ophthalmoscope to enable optimized contrast and enhanced visualization of transparent retinal features.

1. Introduction

Adaptive Optics Scanning Laser Ophthalmoscopy (AOSLO) is a high-resolution retinal imaging technique used to image the living human eye retina with cellular resolution. Conventional confocal AOSLO captures light through a physical aperture placed just before the detector that rejects the signal from out of focus retinal layers, producing high-contrast images of highly reflective layers like the photoreceptors and the nerve fiber layer [1]. However, other retinal cells are transparent, making them more challenging to image. Recent advancements have improved the contrast of these low reflectivity retinal structures by adding off-axis detection to the AOSLO system [2]. The offset detectors collect off-axis light which have likely propagated through less reflective layers of the retina, and which may have been scattered multiple times. Off-axis detectors have been shown to reveal low-reflectivity features such as small capillaries and immune cells. Images obtained using off-axis detection exhibit contrast different to those obtained using the confocal detector. This offset contrast resembles that obtained with differential interference contrast microscopy, a technique that exploits phase variations due to differences in refractive index of the different features of interest. This suggests that the offset contrast in the AOSLO is generated by phase gradients in the retina. While many AOSLO systems worldwide are equipped with offset detection channels, the majority are designed empirically without a model of the light paths. In the literature, Guevara Torres et al. [3] proposed that cells in the retina act like lenses deviating light rays because of the difference of refraction index between the cells and their surrounding medium. This asymmetric distribution of light is then propagated to a deeper layer of the retina which will backscatter it to the detectors. They found that the offset contrast is better when the detector is conjugated to this backscattering deeper layer than with the imaged layer targeted in the confocal channel. Bedggood et al. [4] published a model based on geometrical optics. A consensus on the origin of offset contrast remains elusive, and no wave optics model has been published. We present the first wave optics model to explain offset contrast in AOSLO, alongside numerical simulations for system optimization.

2. Methods

2.1. AOSLO system

In the AOSLO we want to model, a laser diode sends a light beam through the system to focus on a point of the retina. Thanks to two galvanometer scanners (x and y directions), the focused point scans the whole field of view (2° by 2° on the retina) in a raster fashion, allowing us to obtain a 2D image. However, the passage of light through the anterior segment of the eye introduces aberrations that degrade the wavefront reaching the detector. Consequently, the final image is blurred and most of the retinal features cannot be resolved. An adaptive optics arm is therefore added to the system. It works in a closed loop with a Shack-Hartmann wavefront detector that measures the wavefront aberrations and sends a command to a deformable mirror that will change its shape to compensate for these aberrations. Therefore, the wavefront is no longer aberrated and cellular resolution is reached, allowing us to image small retinal features like photoreceptors, nerve fiber bundles or blood cells. The two different detection configurations (confocal and offsets) allow us to see different retinal features in the same acquisition. For example, when observing the nerve fiber layer with the confocal detector, we can simultaneously detect, using the offset detectors, cells that cannot be observed with the confocal detector alone because of their transparency, such as blood cells.

Optical Coherence Imaging Techniques and Imaging in Scattering Media VI, edited by Marinko V. Sarunic, Benjamin J. Vakoc, Yoshiaki Yasuno, Proc. of SPIE-Optica Vol. 13939, 1393917
2025 Published by SPIE-Optica · 1605-7422 · doi: 10.1117/12.3098555

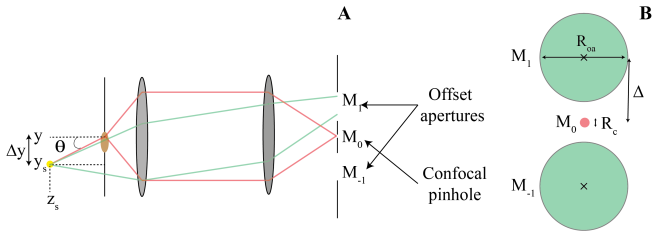

Fig. 1. Overview of the model used for the numerical simulations. A. Optical system with confocal and offset paths of light. The yellow dot is the scatterer and the brown ellipse is the refracting object. B. *En face* view of the detector plane.

2.2. *Numerical simulations*

We start by explaining why, in the first instance, we model only the detection of light emitted by a point source in the sample space (Fig1). This point source emulates the focused illumination interacting with a sub-resolution scatterer. We refer to the field at the detector due to this point source, located in a homogeneous medium, as the detection point spread function (PSF) and denote it as $E_d(\mathbf{r}_s;\mathbf{r}_d)$, where $\mathbf{r}_s = (x_s, y_s, z_s)$ is the location of the point source in the sample space and $\mathbf{r}_d = (x_d, y_d)$ is the position in the detector space. The sample and detector space coordinate systems have their origin at the nominal focal point in each space. Because of the low numerical aperture of the AOSLO, we make a scalar approximation by neglecting the cross-polarised terms arising from a vectorial calculation of the detector field due to an electromagnetic dipole using theory developed by Török *et al.* [5]. When the illumination PSF is incorporated into the model, the field at the detector becomes proportional to $E_i(\mathbf{r}_s)E_d(\mathbf{r}_s;\mathbf{r}_d)$, where $E_i(\mathbf{r}_s)$ is the electric field of the focused illumination incident upon the scatterer.

In practice, scattering regions of tissue can be represented by ensembles of N_{sc} scatterers with positions $\mathbf{r}_{s,j}$. Under the first-order Born approximation, the total field at the detector is given by

$$E_{d,tot}(\mathbf{r}_d) = \sum_{j=1}^{N_{sc}} E_i(\mathbf{r}_{s,j})E_d(\mathbf{r}_{s,j};\mathbf{r}_d) \tag{1}$$

Suppose, however, that the sample contains a refracting object in the vicinity of the focus, as shown in Fig. 1A, which refracts the illumination and invalidates for first-order Born approximation. If the refracting object refracts the beam by an angle θ in the y-direction, the illumination can be approximated by $E_i(\mathbf{r}_s - (0, \theta z_s, 0))$ in the plane $z = z_s$. The effect of this refraction could be investigated by substituting this express into Eq. 1. However, we can gain more physical insight into this system be neglecting the blurring effect of the focussed illumination and approximating Eq. 1 by $E_i((0,0,z_s))E_d((0,\theta z_s, z_s);\mathbf{r}_d)$, since $E_i((0,0,z_s))$ is the field at the centre of the focal spot. We can further simplify this expression by dropping the $E_i((0,0,z_s))$ term, which varies only with z_s. We also make the simplifying assumption that the refracting object is large enough to impart near-uniform refraction of the illumination beam, but small enough such that light returning from the scatterer, located a distance z_s below the refracting object, is insignificantly perturbed. Whilst this assumption is unlikely to be valid when calculting the confocal signal, it is reasonable when calculating the offset aperture signals. Having calculated the field at the detector, it remains only to calculate the AOSLO signals according to:

$$I_i = \int_{-\infty}^{\infty}\int_{-\infty}^{\infty} |E_d((0, z_s\theta, z_s);\mathbf{r}_d)|^2 M_i \mathrm{d}^2\mathbf{r}_d, \tag{2}$$

where M_i represents the different detectors in the system, in particular:

$$M_{\pm 1} = \begin{cases} 1 & \text{if } |\mathbf{r}_d \pm (\Delta, 0)|^2 \leq R_{oa}^2; \\ 0 & \text{otherwise} \end{cases} \qquad M_0 = \begin{cases} 1 & \text{if } |\mathbf{r}_d|^2 \leq R_c^2, \\ 0 & \text{otherwise} \end{cases} \tag{3}$$

where Δ is the separation between offset apertures, R_{oa} is the radius of the offset aperture and R_c is the aperture of the confocal pinhole. We can then calculate two metrics: the differential intensity $I_d = I_{-1} - I_1$ and total offset aperture energy $E = I_{-1} + I_1$. We studied the influence of z_s, Δ and R_{oa} on these metrics. We also note that the conventional AOSLO detection PSF can be calculated by evaluating Eq. 2, but with $E_d(x_s, y_s, z_s)$ in the place of $E_d(0, z_s\theta, z_s)$.

3. Results

Figure 2 shows simulated confocal and offset detector system axial PSFs. We found that when the scatterer is in focus, there is no signal in the offset detectors, as all the energy is concentrated in the confocal detector. However,

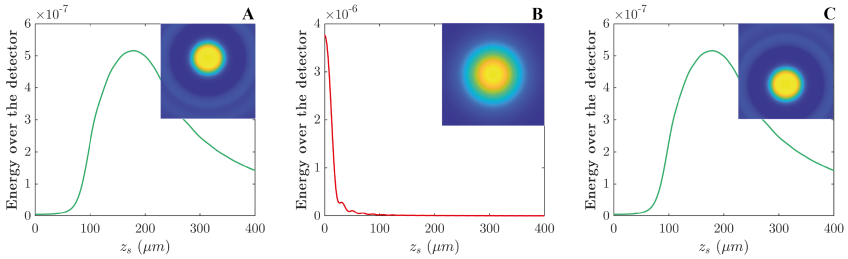

Fig. 2. Influence of the z position of the scatterer on the energy detected on each detector. Insets are the simulated lateral PSF for a scatterer located in the center of the object space, at the defocus position giving the maximum energy ($z_s = 0$ for the confocal detector and $z_s = 180\mu m$ for the offsets). A) North detector. B) Confocal detector. C) South detector.

on moving the scatterer in the z direction, energy in the confocal detector decreases while energy in the offset detectors steadily increases.

Figure 3 shows the offset contrast as a function of the deviation angle for different scatterer defocus (z_s in Fig.1) and for different separation distances of the offset detectors relative to the confocal detector. We find that for each offset configuration, there is a range of deviation angle for which there is a linear relation between the differential intensity and the deviation angle. However, we can see that the proportionality coefficient is not constant but varies with the scatterer defocus and the distance between the offset detectors and the confocal detector.

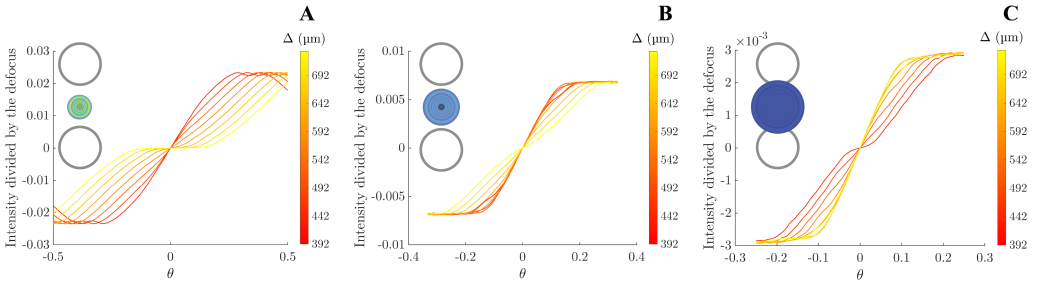

Fig. 3. Evolution of the differential intensity as a function of the deviation angle for different scatterer defocus positions and different offset configurations.A)$z_s = 100\mu m$ B)$z_s = 150\mu m$ C)$z_s = 200\mu m$. The inset images depict sketches of the offset detectors and field intensity of an on-axis scatterer.

4. Conclusion

We developed a model of image formation in AOSLO based on a a 4f configuration. The model was used to determine the AOSLO confocal and offset detector Point Spread Functions. The model was also used to study how differential contrast is influenced by the depth of reflective layers and offset detector separation. Our study suggests that there is indeed a linear relationship between the perceived contrast in offset detectors and the phase gradient imparted by objects such as cells in the focal region. The proportionality coefficient depends on the chosen offset configuration as well as the retinal layer that back illuminates the cells. In the long term, this could enable phase quantitative imaging of the living human retina, allowing us to identify retinal features that are currently visible but not yet well understood.

References

1. A. Roorda, F. Romero-Borja, W. J. Donnelly Iii, H. Queener, T. J. Hebert, and M. C. Campbell, "Adaptive optics scanning laser ophthalmoscopy," *Optics Express*, vol. 10, p. 405, May 2002.
2. D. Scoles, Y. N. Sulai, C. S. Langlo, G. A. Fishman, C. A. Curcio, J. Carroll, and A. Dubra, "In Vivo Imaging of Human Cone Photoreceptor Inner Segments," *Investigative Opthalmology & Visual Science*, vol. 55, p. 4244, July 2014.
3. A. Guevara-Torres, D. R. Williams, and J. B. Schallek, "Origin of cell contrast in offset aperture adaptive optics ophthalmoscopy," *Optics Letters*, vol. 45, p. 840, Feb. 2020.
4. P. Bedggood, Y. Ding, D. Dierickx, A. Dubra, and A. Metha, "Quantification of optical lensing by cellular structures in the living human eye," *Biomedical Optics Express*, vol. 16, p. 473, Feb. 2025.
5. P. Török, P. D. Higdon, and T. Wilson, "Theory for confocal and conventional microscopes imaging small dielectric scatterers," *Journal of Modern Optics*, vol. 45, no. 8, pp. 1681–1698, 1998.